Basic Characteristics of Hemimorphite and Its Transformation Mechanism with Na$_2$CO$_3$

Qihong Wang [1,2], **Xiaolin Zhang** [1,2,*], **Dianwen Liu** [1,2,*], **Shiming Cao** [3], **Kaiwei Song** [1,2], **Man Jing** [2], **Kangkang Li** [2], **Luqing Wu** [2] and **Ruizeng Liu** [1,2]

[1] State Key Laboratory of Complex Nonferrous Meal Resources Clean Utilization, Kunming University of Science and Technology, Kunming 650093, China; wang_qi_hong@126.com (Q.W.); kivy340827@126.com (K.S.); liuruizeng@126.com (R.L.)

[2] Faculty of Land Resource Engineering, Kunming University of Science and Technology, Kunming 650000, China; xkdjingman@163.com (M.J.); kkl163163@163.com (K.L.); aa1321615400@163.com (L.W.)

[3] School of Chemical Engineering & Technology, China University of Mining and Technology, Xuzhou 221000, China; ironshark@163.com

*   Correspondence: xiaolin6001@sina.com (X.Z.); dianwenliu@kmust.edu.cn (D.L.)

Abstract: The crystal of hemimorphite is a non-conductor. The Si–O bond in the crystal is strong, whereas the Zn–O bond is weak. These properties lead to the easy breakage of the Zn–O bond in the crushing process of hemimorphite. Thus, the interaction between minerals and polar water molecules is strong, and natural floatability of ores is poor. This study systematically investigated the characteristics of hemimorphite and its action mechanism with Na$_2$CO$_3$. Results of SEM-EDS showed that the surface of hemimorphite dissolved after interacting with Na$_2$CO$_3$, and the contents of Si and O decreased, whereas Zn and C increased. XPS analysis showed that the carbonate group was detected. The interaction between CO$_3{}^{2-}$ and hemimorphite was calculated using the first principles calculation based on density functional theory. The results indicate that an O atom in CO$_3{}^{2-}$ interacted with Zn^{2+} from the (100) plane of hemimorphite. The interaction between Zn and O atoms was not strong, and the Zn atoms were not completely displaced, which was proven by density of state analysis and the EDS and XPS results. The Mulliken population showed that the O–Zn bond was the atomic bonding of CO$_3{}^{2-}$ with Zn^{2+} and exhibited properties of ionic bonds. Thus, hemimorphite transformed to smithsonite-like mineral (ZnCO$_3$) when acting with CO$_3{}^{2-}$.

Keywords: sodium carbonate (Na$_2$CO$_3$); hemimorphite; transformation mechanism; smithsonite-like mineral

1. Introduction

Zinc oxide ore is an important zinc mineral resource that is accompanied with technical problems during actual separation because of its various mineral resources, inlay complexity, and high soluble salt content [1,2]. Minerals are easily slimed and lead to heavy metal loss. Mineral surfaces contaminated with other minerals are not easy to mineralize into monomers [3]. In the application of zinc oxide ore flotation reagents, Dong et al. [4] from Hunan Research Institute of nonferrous metals used advanced xanthate and chelating collectors for the beneficiation of complex zinc oxide ore, and a good concentrate index was obtained. Zhou et al. [5] used sodium fluorosilicate and sodium silicate as inhibitors of gangue minerals which effectively promoted the recovery of zinc oxide ore. The recovery of oxidized zinc ores is usually carried out by flotation when fatty amines are used as collectors. This techniques characterized by the consumption of large amounts of reagents, and careful optimization of reagent proportion is needed [6].

To study hemimorphite activation, some researchers [7] conducted calculations of radical electronegativity and ultraviolet band spectrochemical analysis and used a series of analytical methods. They found that N and O atoms in α-nitroso-β-naphthol generate a corresponding chelate, which is a compound with Zn^{2+}, on mineral surfaces upon the occurrence of bonding interactions. When α-nitroso-β-naphthol is used as an activating agent, the hydrophobicity of minerals is enhanced. Chen et al. [8] of Guangxi University found that OH^- and HS^- both exert an activation effect on hemimorphite. An obvious synergistic effect was observed in the pH range of 9–11. The "Na_2S-Pb(II)-xanthate" process can be successfully used for the flotation of hemimorphite, increasing the recovery rate from 40% to 90%. PbS is generated when an ion exchange mechanism occurs between Pb(II) and ZnS, as proven by X-ray diffraction results [9]. Similar effects of Pb(II) on hemimorphite were also observed in the sodium oleate flotation system [10]. Besides, mechanical activation significantly influences the physicochemical properties of hemimorphite, such as morphologies, crystal structures, and particle size distributions [11].

The present study aimed to investigate the characteristics of hemimorphite and its transformation mechanism with Na_2CO_3. SEM-EDS and XPS were conducted to analyze the surface morphology, elemental changes and chemical states in minerals. We used computer simulation techniques to model the transformation of CO_3^{2-} on hemimorphite. The results can provide important insight into the transformation mechanism of CO_3^{2-} on hemimorphite.

2. Experimental

2.1. Materials and Reagents

The hemimorphite sample used in these experiments was collected from Lanping in Yunnan Province, China. For transform experiments, the hemimorphite sample was crushed and dry ground in an agate mortar. Ground products were sieved to achieve a particle fraction of −74 μm accounts for 85%. Multi-elements analysis showed that the sample contained 53.81% Zn, which indicated high purity except for low levels of mineral impurities. X-ray diffraction (XRD) (Shimadzu, Kyoto, Japan) pattern of samples shown in Figure 1, hemimorphite crystal was observed, and the diffraction peak is consistent with the data presented in the JCPDS card. Analytical-grade Na_2CO_3 and $NaOH/H_2SO_4$ were employed as activator and regulator, respectively. Pure deionized water with a resistivity of 18 MΩ obtained from a Milli-Q5O system (Billerica, MA, USA) was used in these experiments.
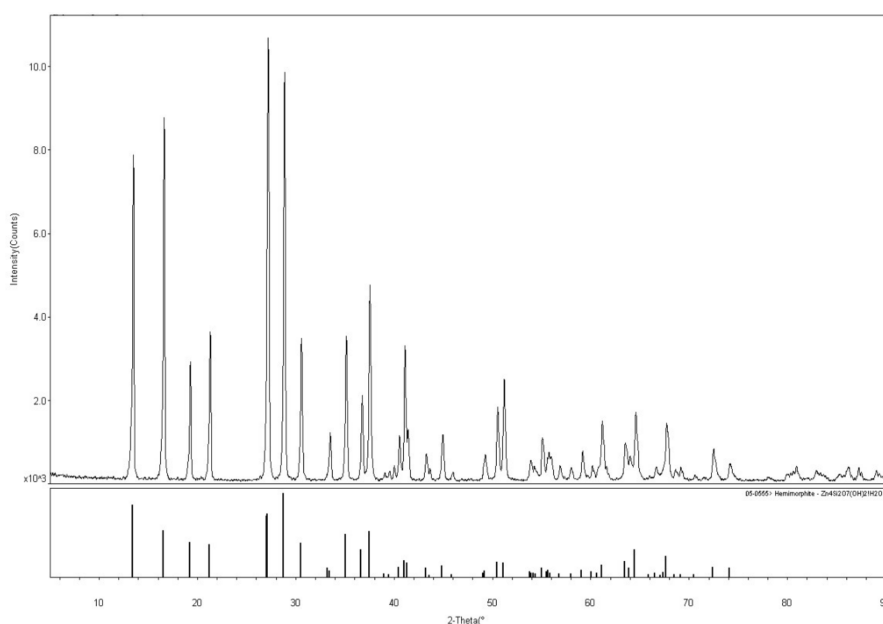
Figure 1. X-ray diffraction (XRD) pattern of the pure hemimorphite samples.

2.2. SEM-EDS Analysis

Before and after acting with Na_2CO_3, the surface morphology and composition of the hemimorphite were examined by SEM-EDS under the Jeol JSM-6360 instrument (JEOL, Tokyo, Japan) at 20 kV.

2.3. XPS Analysis

The XPS measurements were performed using PHI5000 Versa Probe II (ULVAC-PHI, Chigasaki-shi, Japan) equipped with a monochromatic Al Kα X-ray source. The analyzed sample was first subjected to a survey scan to identify chemical components, followed by high-resolution scans on a certain element. Carbon is ubiquitous and is present on all surfaces for XPS analysis. Thus, all spectra were calibrated using the carbon 1s spectral peak at 284.8 eV.

2.4. Computational Methods

Calculations in this article were conducted using Cambridge Serial Total Energy Package developed by Payneet al. [12]. This software package is the first-principle method based on density functional theory (DFT). Hemimorphite is a nesosilicate mineral and an orthorhombic system [13,14]. It contains a 3D spatial skeleton formed by a connected vertex between Si–O double tetrahedra and Zn–O tetrahedra in its crystal structure. The three corners of the tetrahedron are bonded together and form a six-atomic ring (2Zn + Si + 3O), which is connected with each other on the (010) surface to form an unlimited extension of the layer. The electronic structure of the ore was calculated via DFT [15,16], and the optimized crystal cell model is shown in Figure 2.
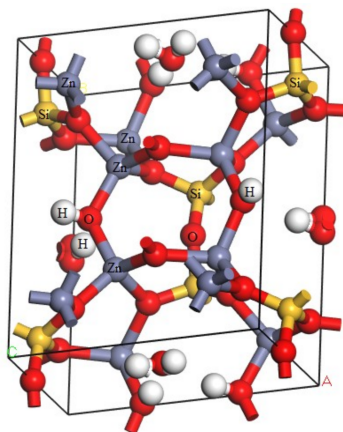

Figure 2. Cell model of hemimorphite.

3. Results and Discussion

3.1. Analysis of Energy Band Structure and Density of States of Hemimorphite

Energy band theory [17,18] can be used to qualitatively explain the motion characteristics of electrons in the crystal structure. The energy band structure of hemimorphite (Figure 3) mainly consists of three parts, conduction band (3.3 eV to 11.5 eV), valence band (−17.4 eV to −16.5 eV), and filled band (−8.5 eV to 0.68 eV). The conduction band is conductive, whereas the position in the filled band is full of electrons and does not show electrical conductivity. The valence band is occupied by the valence electron. The electronic movement as a whole is symmetrical when produced by the external force, and neither has electrical property. By contrast, electrical properties are exhibited when the motion of the electron is asymmetric. The energy band gap was analyzed, which demonstrated that the energy band gap of hemimorphite was 3.336 eV, differing greatly from another zinc oxide ore [19], but it was close to that of smithsonite (3.529 eV) [20]. These properties indicate the weak

electron mobility and poor conductivity of hemimorphite. Figure 4 presents the density of states of hemimorphite. The energy band was divided into four parts in the range of −19.7 eV to 11.0 eV. The valence band from −17.4 eV to 16.5 eV was mainly composed of the s orbitals and p orbitals, which also contributed to the density of states of hemimorphite. The valence band, which ranged from −8.5 eV to −7.1 eV, was mainly made up of p orbitals and s orbitals, and most of them were p orbitals. The valence band mainly consisted of d and p orbitals in the range of −7.1 eV to 0.68 eV, and the s orbitals contributed as well. In addition, the conduction band energy level was mainly composed of p and s orbitals, and the contributions of the two orbitals did not considerably differ. The density of states near the Fermi level was made up primarily of p and d orbitals, which indicated that this crystal was a non-conductor. These results were consistent with the findings of energy band analysis.
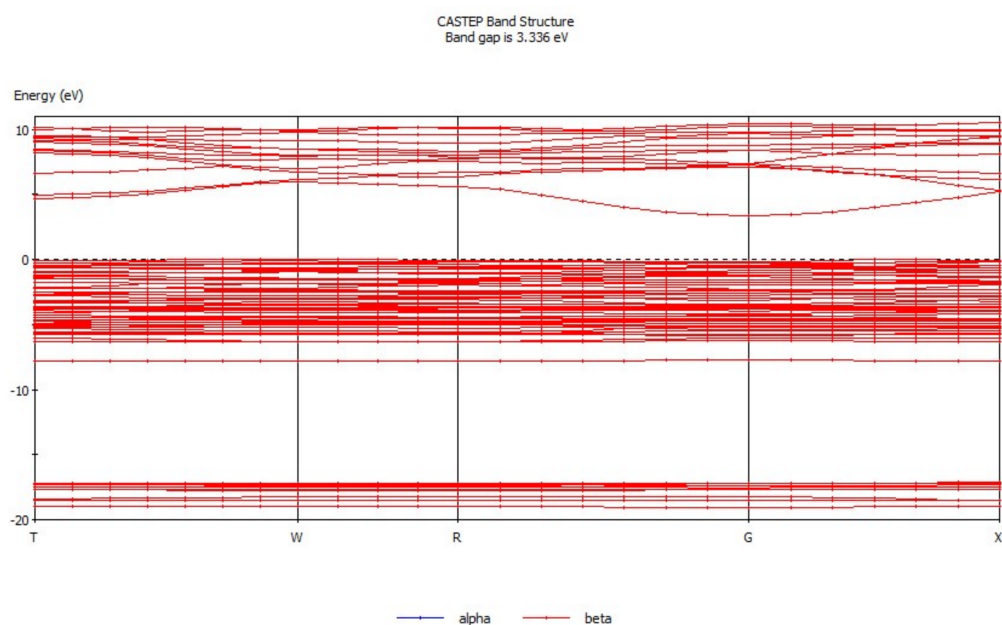
Figure 3. Energy band diagram of hemimorphite.
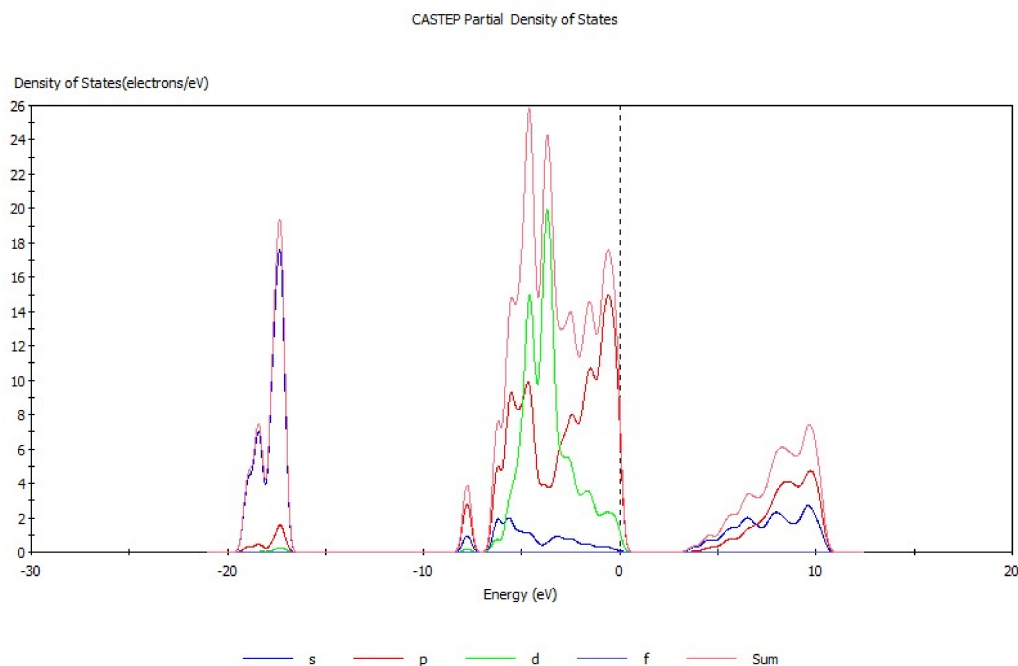
Figure 4. Partial densities of states of hemimorphite.

3.2. Mulliken Population Analysis

Mulliken population is a method used to describe the distribution of electric charge between the correlated atoms, and it can demonstrate the charge distribution, transfer, bonding, and other information in a simulated system [21–24]. Professor Hu [25] proposed that bond energy E_{AB} considers the population of overlapping atomic orbitals and different contributions caused by varying levels in the molecular orbital. The present study only analyzed the influence of the Mulliken population on bond energy intensity. The Mulliken population was successfully applied to the S_N2 reaction with resonance theory by Ikeda et al. [26]. When the Mulliken population of bonds is large, the covalent bond between atoms is strong; if it is small, there is minimal overlap of electronic clouds and bond covalency is weak. The bond between atoms is ionic when the Mulliken population is low [27–29]. The Mulliken population of hemimorphite is presented in Table 1, which shows that the bond length of Si–O was 1.6153 Å (average value). The population was 0.5975 (average value), and its covalency was strong. The bond length of Zn–O was 1.9529 Å (average value), and the population was 0.36 (average value). Therefore, ionicity for its covalency was weaker than that of the Si–O bond. Kaupp et al. [30] also reported further details in his research on bond length/bond strength.

Table 1. Mulliken population value of partial bonds of hemimorphite.

Bond	Population	Spin	Length (Å)	Bond	Population	Spin	Length (Å)
O 004–Si 001	0.62	0.00	1.60910	O 005–Zn 001	0.40	0.00	1.94416
O 003–Si 002	0.62	0.00	1.60910	O 006–Zn 002	0.40	0.00	1.94416
O 001–Si 001	0.62	0.00	1.60910	O 005–Zn 004	0.40	0.00	1.94416
O 002–Si 002	0.62	0.00	1.60910	O 006–Zn 003	0.40	0.00	1.94416
O 009–Si 002	0.56	0.00	1.62123	O 003–Zn 004	0.33	0.00	1.96457
O 009–Si 001	0.56	0.00	1.62123	O 002–Zn 001	0.33	0.00	1.96457
O 006–Si 002	0.59	0.00	1.62158	O 001–Zn 002	0.33	0.00	1.96457
O 005–Si 001	0.59	0.00	1.62158	O 004–Zn 003	0.33	0.00	1.96457
O 001–Zn 001	0.36	0.00	1.93171	O 008–Zn 004	0.35	0.00	1.97100
O 004–Zn 004	0.36	0.00	1.93171	O 007–Zn 003	0.35	0.00	1.97100
O 003–Zn 003	0.36	0.00	1.93171	O 007–Zn 001	0.35	0.00	1.97100
O 002–Zn 002	0.36	0.00	1.93171	O 008–Zn 002	0.35	0.00	1.97100

### 3.3. Charge Density Difference of Hemimorphite

The analysis of the charge density difference of atoms revealed information on atomic bonding and gain and loss of electrons [31]. As shown in the charge density difference map of hemimorphite in Figure 5, the blue region represents electron deficiency, the red area represents the electron concentration, and the white area shows minimal changes in electron density. The charge density difference of the Si–O bond is illustrated on the left side of Figure 4, whereas the right part illustrates the charge density difference of the Zn–O bond. The Si–O bond was covalent due to the large overlap of electron cloud between Si–O atoms in the internal structure of the crystal of hemimorphite. By contrast, the Zn–O bond showed iconicity because its degree of overlap was small with a low inter-atomic force. The floatability of minerals can be greatly influenced by their surface bond energy [32]. Minerals with weak covalency and strong iconicity demonstrate strong hydrophilicity but good floatability. Given that the Si–O bond in hemimorphite was very strong, the Zn–O bond was often broken during crushing and grinding, resulting in the high presence of the Zn–O bond on the exposed mineral surface. The Zn–O bond exhibited strong ionicity and weak covalency, so minerals often showed a strong force with polar water molecules; this phenomenon was the reason for the poor flotability of hemimorphite. Ore is easily slimed during crushing and separating if the proportion of Si in the mineral composition is high, leading to minerals being hard to separate effectively [33,34]. Thus, high-silicon hemimorphite was also difficult to separate.

(**a**)   (**b**)
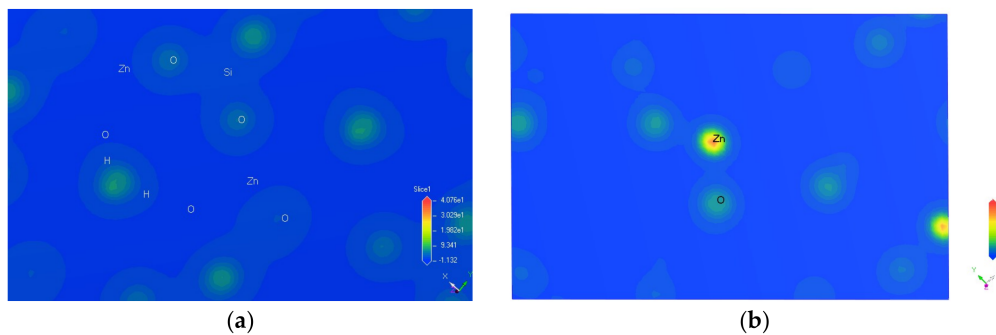
Figure 5. Charge density difference map of hemimorphite. (**a**) Si–O bond; (**b**) Zn–O bond.

3.4. Transformation Mechanism of CO_3^{2-} on Hemimorphite

The hemimorphite surface was analyzed by SEM-EDS before and after treatment with Na_2CO_3 (Figure 6). Cao's research has proved that the floatability of hemimorphite behaves well when pH = 10.0 [35]. Thus, transform experiment was carried out when Na_2CO_3 (1×10^{-3} mol/L) as activator, and the pulp pH was adjusted to pH = 10.0 by $NaOH/H_2SO_4$ with 3 minutes treatment. Before the reaction, the dissociation surface of pure minerals was relatively flat with a pebble-like texture; the mineral surface turned concave and convex and exhibited breccias after the reaction. Thus, Na_2CO_3 exerted significant dissolution to the surface of hemimorphite. EDS analysis revealed that the contents of O and Si on the surface of hemimorphite decreased, whereas Zn and C increased after the reaction with Na_2CO_3. Elemental Si and O in hemimorphite mainly existed in the form of $Si_2O_7^{6-}$, so the decrease in the contents of O and Si was caused by the micro dissolution of $Si_2O_7^{6-}$ in solution. Simultaneously, the dissolution of $Si_2O_7^{6-}$ led to the increase in bare Zn^{2+} on the surface of hemimorphite, which increased the Zn content. Furthermore, the significant increase in the C content was mainly due to the combination with bare Zn^{2+} and then transformed smithsonite-like minerals that were not identical. As seen in the Table 2, the carbon content increased from 0.60% to 3.61% after acting, however, is still at a low level.
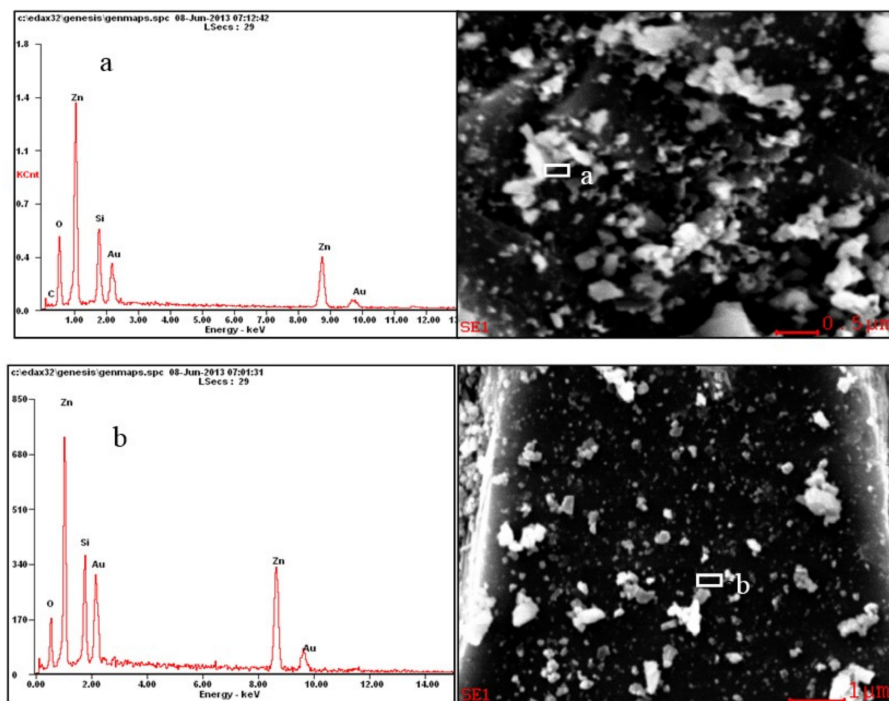
Figure 6. Energy dispersive spectroscopy of hemimorphite before (**a**) and after (**b**) reaction with Na_2CO_3.

**Table 2.** EDS analysis of selected particles of hemimorphite in a and b.

Element	wt (%)		At (%)	
	a (Before Adsorption)	b (After Adsorption)	a (Before Adsorption)	b (After Adsorption)
CK	00.60	03.61	02.02	14.11
OK	19.06	08.10	47.87	23.74
SiK	11.53	04.93	16.50	08.24
ZnK	47.63	70.99	29.29	50.96
AuL	21.18	12.37	04.32	02.95

3.5. XPS Measurements for the Transformation of CO_3^{2-} on Hemimorphite

The C element content on the surface of hemimorphite is still at a low level after acting with Na_2CO_3 analyzed by EDS. Thus, XPS was employed in this study for further explaining the existence of CO_3^{2-} on hemimorphite surfaces treated with the Na_2CO_3 concentration of 1×10^{-3} mol/L because XPS is a useful tool for directly detecting the elemental compositions and chemical states of interaction products [36–38].

The C1s spectra of the treated and untreated hemimorphite sample with Na_2CO_3 are plotted in Figure 7. As shown in Figure 7a, the C1s peaks located at the binding energy values of 284.8 eV, 286.45 eV and 289.05 eV were attributed to the hydrocarbon and carbon–oxygen contaminants. The C1s peak in Figure 7b has a certain change due to the instrument deviation, corresponding to the 284.8 eV, 286.28 eV and 288.73 eV. As a result, the substantial contribution of C1s peaks to the transformed hemimorphite samples may be represented by the binding energy values of 289.59–289.26 eV [36,37], corresponding to the 289.75 eV in Figure 7b, which is associated with the carbonate group. Some effects has occurred between CO_3^{2-} and hemimorphite, while the intensity of carbonate group in 289.75 eV is relatively low.
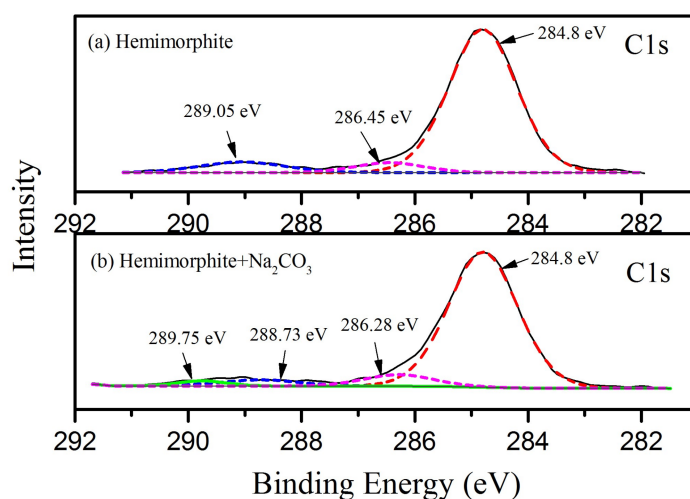

Figure 7. XPS Analysis for the treated and untreated hemimorphite with Na_2CO_3. (**a**) hemimorphite; (**b**) hemimorphite + Na_2CO_3.

3.6. Analysis of Density of States of Hemimorphite after Interacting with CO_3^{2-}

To further prove the possibility of the existence of the above mentioned smithsonite-like minerals, the relationship between CO_3^{2-} and hemimorphite was calculated based on the first principles of DFT [39]. Figure 8 illustrates the transformation model before and after the reaction of hemimorphite. Calculations demonstrated carbon and oxygen atoms in CO_3^{2-} tethered through a C–O single bond, in which one oxygen (red part) interacted with Zn^{2+} (grey section) from the (100) plane of hemimorphite.
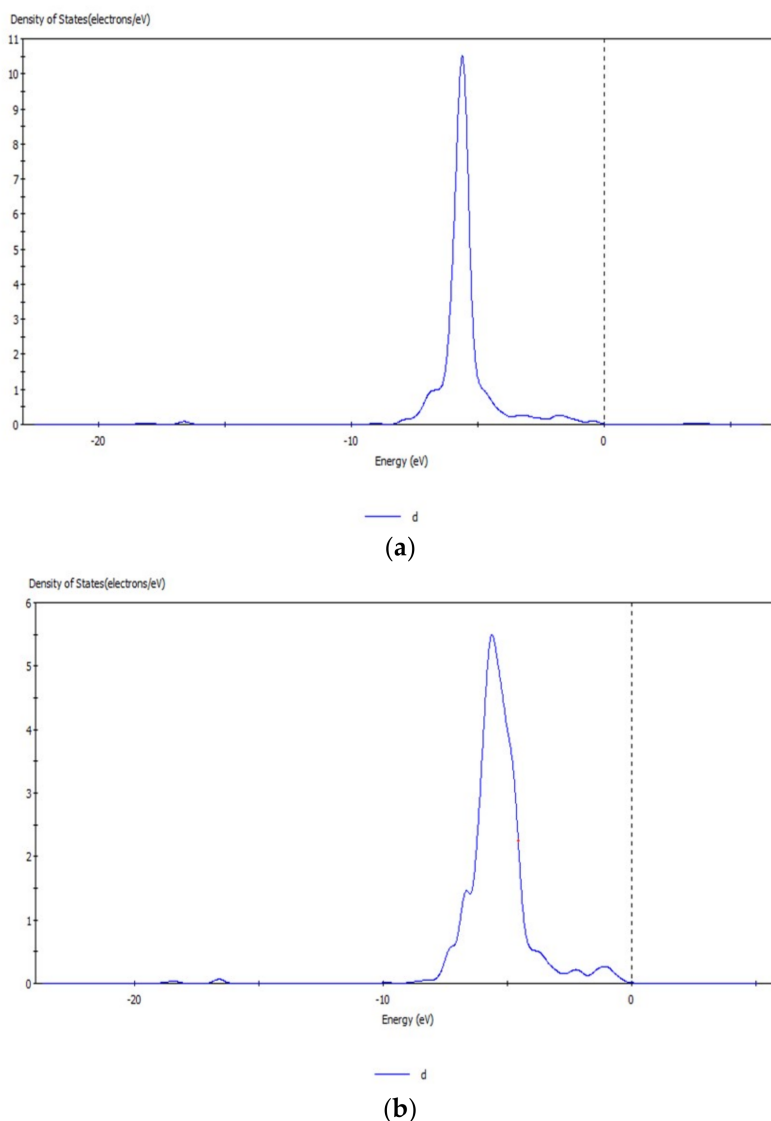
The results of the analysis of density of states of Zn and CO_3^{2-} are depicted in Figures 9 and 10 before and after the interaction.
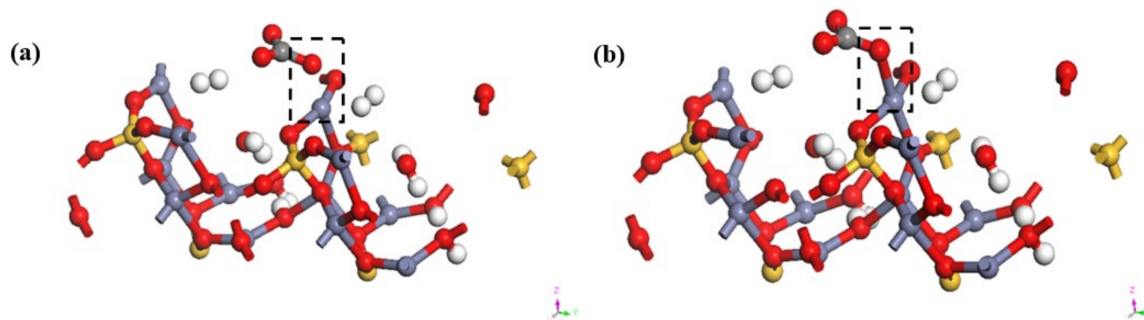
Figure 8. Transformation of initial (**a**) and final (**b**) states of CO_3^{2-} on the surface of the hemimorphite.

(**a**)

(**b**)
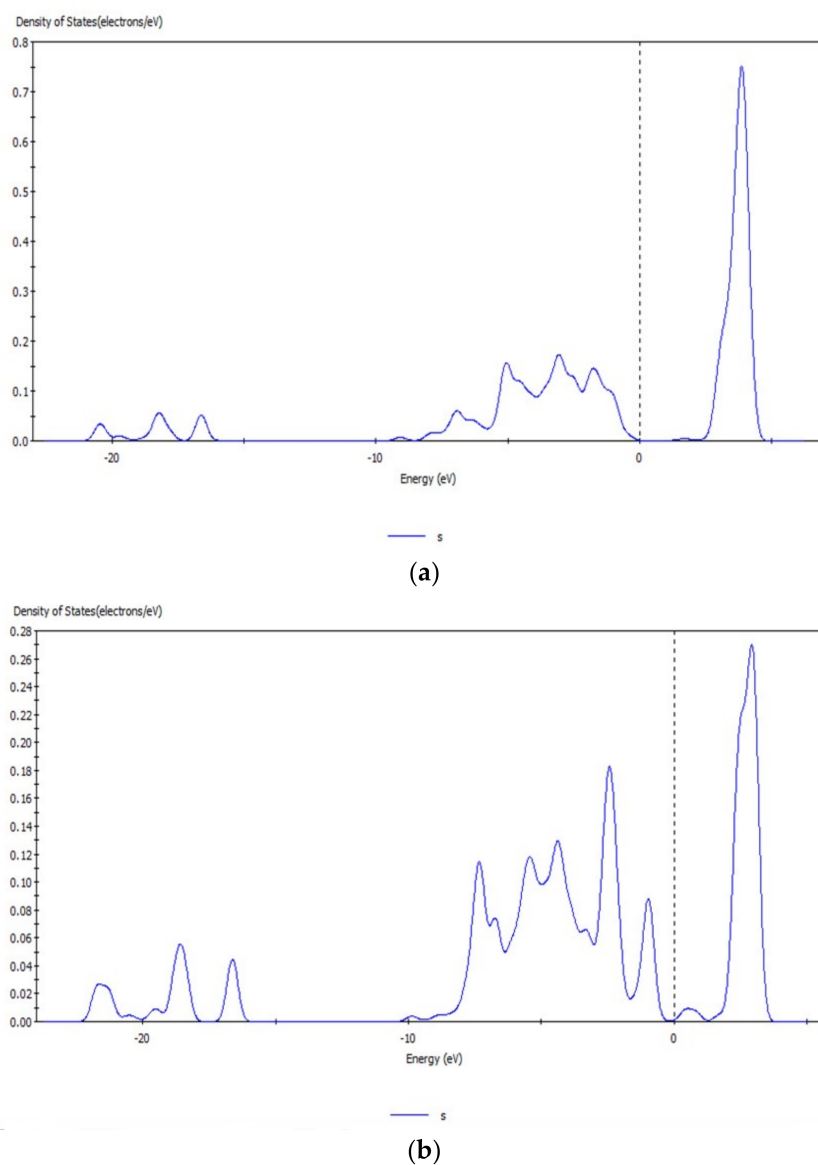
Figure 9. s orbital before (**a**) and after (**b**) transformation of CO_3^{2-} with hemimorphite.

(**a**)

(**b**)

Figure 10. d orbital before (**a**) and after (**b**) transformation of CO_3^{2-} with hemimorphite.

The peak values of the s and d orbitals of the Zn atom were reduced after reaction, and the density of states of the d orbital at -5.63 eV decreased obviously by 5.0 eV by comparing the peak values of density of states before and after transformation with CO_3^{2-}. The d orbital of Zn atom lost electrons, and a new density of states arose at -6.65 eV, which indicated that the electrons in the d orbital were involved in the bond-forming reactions. However, no significant change was observed in the localization of s and d orbitals and their peaks. Thus, the bond between Zn–O was not strong, and Zn atoms on the surface were not completely substituted. Simultaneously, the reaction between Zn^{2+} and CO_3^{2-} transformed smithsonite-like minerals ($ZnCO_3$); the surface of hemimorphite demonstrated similar properties to smithsonite-like minerals.

The bond length formed by the transformation of CO_3^{2-} on hemimorphite was 2.159 Å after calculation (see Figure 11). Compared with the Mulliken population of hemimorphite after reaction whose bond length of O 029–Zn 011 was 2.15893 Å (Table 3, red box), both values were very close. The Zn–O bond was formed by CO_3^{2-} and Zn^{2+}, whose Mulliken population value was 0.21. We observed an overlap of electronic cloud between atoms, which demonstrated the bonding states. Its value was relatively small, and the covalent bond was weak compared with the other O–Zn

bond. Therefore, the property of the ionic bond was exhibited, which was consistent with the results of the analysis of density of states.
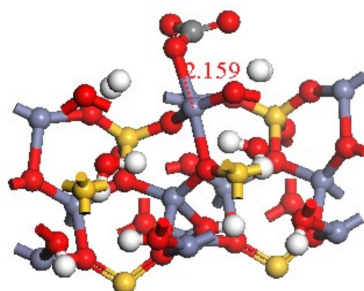

Figure 11. Bond length of Zn–O.

Table 3. Mulliken population value of partial bonds of hemimorphite after acting.

Bond	Population	Spin	Length (Å)
O 024–Zn 006	0.22	0.00	2.11216
O 005–Zn 006	0.18	0.00	2.12877
O 029–Zn 011	0.21	0.00	2.15893
O 016–Zn 009	0.11	0.00	2.16948
O 014–Zn 007	0.14	0.00	2.17600

4. Conclusions

The crystal of hemimorphite is a non-conductor because the density of states near the Fermi level is composed of p and d orbitals. Hemimorphite exhibits a large band gap between the valence band and conduction band. Poor abilities of electron transport and conductivity of hemimorphite were proven by unit cell modeling and band structure analysis. The Mulliken population value of the Si–O bond was larger than that of the Zn–O bond, indicating strong covalency. Therefore, the Zn–O bond was mostly broken during rushing, and Zn–O and Zn^{2+} were exposed on the mineral surface. The interaction between hemimorphite and polar water molecules was strong due to the strong ionicity and weak covalency of the Zn–O bond, which demonstrated good hydrophilicity. This interaction was one of the reasons why hemimorphite was difficult to separate.

The EDS analysis showed that the carbon content on hemimorphite increased from 0.60% to 3.61%, and XPS result revealed the carbonate group was detected at the binding energy values of 289.75 eV after acting.

One oxygen in CO_3^{2-} interacted with Zn^{2+} from the (1 0 0) plane of hemimorphite, as indicated by the transformation model and its new peak of density of states of the d orbital. The bonding reaction was observed through the analysis of density of states. The position of the Zn–O bond should be in O 029–Zn 011, corresponding to the population of 0.21, which suggested the ionic bonds. Furthermore, the reaction between CO_3^{2-} and Zn^{2+} was considered to transform a smithsonite-like mineral ($ZnCO_3$).

Author Contributions: Xiaolin Zhang, Dianwen Liu conceived and designed the experiments; Shiming Cao and Qihong Wang performed the experiments; Xiaolin Zhang, Shiming Cao, Qihong Wang, Kaiwei Song, Man Jing, Kangkang Li, Luqing Wu and Ruizeng Liu analyzed the data; Qihong Wang wrote this paper and Dianwen Liu corrected it.

Conflicts of Interest: The authors declare no conflict of interest.

References

1.　Yan, L.G.; Wang, A.J.; Chen, Q.S.; Li, J.W. Dynamic material flow analysis of zinc resources in China. *Resour. Conserv. Recycl.* **2013**, *75*, 23–31. [CrossRef]
2.　Zhang, X.F.; Hu, Y.H.; Sun, W.; Xu, L.H. The Effect of Polystyrene on the Carrier Flotation of Fine Smithsonite. *Minerals* **2017**, *7*, 52. [CrossRef]
3.　Dai, S.F.; Chou, C.L.; Finkelman, R.B.; Seredin, V.V.; Zhou, Y.P. Geochemistry of trace elements in Chinese coals: A review of abundances, genetic types, impacts on human health, and industrial utilization. *Int. J. Coal Geol.* **2012**, *94*, 3–21. [CrossRef]
4.　Dong, Y.H. Mineral Processing Research on a Complicated Refractory Zinc Oxide Ore. *Hunan Nonferrous Met.* **2015**, *31*, 23–26. (In Chinese)
5.　Zhou, Q.; Yang, Y.Z.; Liang, Y.Q. Study on Mineral Processing Technology for Refractory Zinc Oxide Ore. *Min. Metall. Eng.* **2014**, *34*, 54–57. (In Chinese)
6.　Pereira, C.A.; Peres, A.E.C. Reagents in calamine zinc ores flotation. *Miner. Eng.* **2005**, *18*, 275–277. [CrossRef]
7.　Zhou, W. Study on Activation Behavior of α-Nitroso-β-Naphthol in Flotation of Hemimorphite. Master's Thesis, Hunan University, Changsha, China, 2010; pp. 35–40. (In Chinese)
8.　Chen, Y.; Chen, J.H.; Wu, B.Z.; Mu, X.; Wei, Z.W. Effect of synergism between hydroxy radical and sulfhydryl radical on the amine flotation of hemimorphite. *Met. Mine* **2009**, *39*, 65–68. (In Chinese)
9.　Jia, K.; Feng, Q.M.; Zhang, G.F.; Shi, Q.; Chang, Z.Y. Understanding the roles of Na_2S and Pb(II)in the flotation of hemimorphite. *Miner. Eng.* **2017**, *111*, 167–173. [CrossRef]
10.　Liu, C.; Feng, Q.M.; Zhang, G.F.; Ma, W.K.; Meng, Q.Y.; Chen, Y.F. Effects of lead ions on the flotation of hemimorphite using sodium oleate. *Miner. Eng.* **2016**, *89*, 163–167. [CrossRef]
11.　Yuan, T.C.; Cao, Q.Y.; Li, J. Effects of mechanical activation on physicochemical properties and alkaline leaching of hemimorphite. *Hydrometallurgy* **2010**, *104*, 136–141.
12.　Payne, M.C.; Teter, M.P.; Allan, D.C.; Arias, T.A.; Joannopoulos, J.D. Iterative minimization techniques for ab initio total-energy calculations: Molecular dynamics and conjugate gradients. *Rev. Mod. Phys.* **1992**, *64*, 1045–1097. [CrossRef]
13.　Seryotkin, Y.V.; Bakakin, V.V. Structural evolution of hemimorphite at high pressure up to 4.2 Gpa. *Phys. Chem. Miner.* **2011**, *38*, 679–684. [CrossRef]
14.　Validžić, I.L.; Mitrić, M.; Jokić, B.M.; Čomor, M.I. Structural and optical characterization of hemimorphite with flower-like morphology synthesized by a novel low-temperature method. *Mater. Lett.* **2012**, *85*, 138–141. [CrossRef]
15.　Mao, M.; Li, Z.; Pan, Y. Phase transitions and proton ordering in hemimorphite: New insights from single-crystal EPR experiments and DFT calculations. *Phys. Chem. Miner.* **2012**, *40*, 133–143. [CrossRef]
16.　Topsakal, M.; Cahangirov, S.; Bekaroglu, E.; Ciraci, S. A first-principles study of zinc oxide honeycomb structures. *Phys. Rev. B* **2009**, *80*, 235119. [CrossRef]
17.　Guo, L.Q.; Wu, H.N.; Liu, J.H.; Ma, H.; Song, K.Y.; Li, D.Y. Density Functional theory study on energy band and density of states of ZnO. *J. Synth. Cryst.* **2009**, *2*, 440–444. (In Chinese)
18.　Iokibe, K.; Sakamoto, T.; Tachikawa, H.; Azumi, K. Density functional theory study of zinc clusters. *J. Surf. Finish. Soc. Jpn.* **2009**, *60*, 592–597. [CrossRef]
19.　Mohamad, A.A.; Hassan, M.S.; Yaakob, M.K.; Taib, M.F.M.; Badrudin, F.W.; Hassan, O.H.; Yahya, M.Z.A. First-principles calculation on electronic properties of zinc oxide by zinc–air system. *J. King Saud Univ. Eng. Sci.* **2017**, *29*, 278–283. [CrossRef]
20.　Wu, D.D. Research on Ammonium Salton Strengthen Suifide Flotation Theory for Smithsonite. Ph.D. Thesis, Kunming University of Science and Technology, Kunming, China, 2015; pp. 60–69. (In Chinese)
21.　Wu, L.; Hou, T.J.; Wang, Y.; Zhao, Y.F.; Guo, Z.Y.; Li, Y.Y.; Lee, S.T. First-principles study of doping effect on the phase transition of zinc oxide with transition metal doped. *J. Alloys Compd.* **2012**, *541*, 250–255. [CrossRef]
22.　Shaik, S. A personal story on a renaissance in valence bond theory: A theory coming of age! *Comput. Theor. Chem.* **2017**, *2*, 1–30. [CrossRef]
23.　Andrés, R.B.M.; Florentino, L.U.; Mauricio, T.; Humberto, T. Effect of impurities on the electronic and magnetic properties of zinc oxide nanostructures. *Chem. Phys. Lett.* **2010**, *492*, 82–88.
24.　Magnasco, V. Chapter 15: Valence bond theory and the chemical bond. In *Elementary Methods of Molecular Quantum Mechanics*; Elsevier: Amsterdam, The Netherlands, 2013; pp. 599–680.

25. Hu, Z.Q. Molecular orbital theory studies on bond energy I. theoretic equation. *Acta Chim. Sin.* **1998**, *56*, 353–358. (In Chinese)

26. Ikeda, A.; Nakao, Y.; Sato, H.; Sakaki, S. A resonance theory consistent with Mulliken-population concept. *Chem. Phys. Lett.* **2011**, *505*, 148–153. [CrossRef]

27. Ogorodnikova, N.A. On invariance of the Mulliken substituent-induced charge changes in quantum-chemical calculations of different levels. *J. Mol. Struct. THEOCHEM* **2009**, *894*, 41–49. [CrossRef]

28. Magnasco, V. Chapter 10: Valence bond theory and the chemical bond. In *Elementary Methods of Molecular Quantum Mechanics*; Elsevier: Amsterdam, The Netherlands, 2007; pp. 473–575.

29. Pipek, J. Unique positive definite extension of Mulliken's charge populations of non-orthogonal atomic basis functions. *J. Mol. Struct. THEOCHEM* **2000**, *501–502*, 395–401. [CrossRef]

30. Kaupp, M.; Danovich, D.; Shaik, S. Chemistry is about energy and its changes: A critique of bond-length/bond-strength correlations. *Coord. Chem. Rev.* **2017**, *344*, 355–362. [CrossRef]

31. Gunnarsson, O.; Jones, R.O. Self-interaction corrections in the density functional formalism. *Solid State Commun.* **1981**, *37*, 249–252. [CrossRef]

32. Gao, Z.Y.; Sun, W.; Hu, Y.H. Mineral cleavage nature and surface energy: Anisotropic surface broken bonds consideration. *Trans. Nonferrous Met. Soc. China* **2014**, *24*, 2930–2937. [CrossRef]

33. Ren, S.P.; Tong, X.; Zhou, Y.C. Study and application of desilication process in mineral processing. *Min. Metall.* **2013**, *22*, 32–36. (In Chinese)

34. Ejtemaei, M.; Gharabaghi, M.; Irannajad, M. A review of zinc oxide mineral beneficiation using flotation method. *Adv. Colloid Interface Sci.* **2014**, *206*, 68–78. [CrossRef] [PubMed]

35. Wang, Q.H.; Zhang, X.L.; Jing, M.; Rao, F.; Wu, L.Q.; Li, K.K.; Cao, S.M. A review of forming process and flotation mechanism of hemimorphite. *Chin. J. Process Eng.* **2017**, *17*, 903–910. (In Chinese)

36. Feng, Q.C.; Zhao, W.J.; Wen, S.M.; Cao, Q.B. Activation mechanism of lead ions in cassiterite flotation with salicylhydroxamic acid as collector. *Sep. Purif. Technol.* **2017**, *178*, 193–199. [CrossRef]

37. Feng, Q.C.; Wen, S.M.; Deng, J.S.; Zhao, W.J. Combined DFT and XPS investigation of enhanced adsorption of sulfide species onto cerussite by surface modification with chloride. *Appl. Surf. Sci.* **2017**, *425*, 8–15. [CrossRef]

38. Feng, Q.C.; Zhao, W.J.; Wen, S.M. Surface modification of malachite with ethanediamine and its effect on sulfidization flotation. *Appl. Surf. Sci.* **2018**, *436*, 823–831. [CrossRef]

39. Yadav, S.K.; Sadowski, T.; Ramprasad, R. Density functional theory study of ZnX (X = O, S, Se, Te), under uniaxial strain. *Phys. Rev. B* **2010**, *81*, 144120. [CrossRef]